Locating the gamma-ray emission regions in the relativistic jet of 3C 279.

Tekano Mbonani, Brian van Soelen & Richard Britto

Department of Physics

University of the Free State

High Energy Astrophysics in Southern Africa 2024

2 – 4 October 2024

mbonanits@ufs.ac.za | www.ufs.ac.za

UNIVERSITY OF THE FREE STATE

Outline

- Introduction: 3C 279
- Optical and Gamma-ray Data
- Results:
  - The z-transformed discrete cross-correlation functions: Time-lags
  - Gamma-ray flux temporal profiling
  - Physical Constraints: Doppler factors, emission region radii and distance from the SMBH.
  - Gamma-ray SED: spectral energy breaks
- Discussion

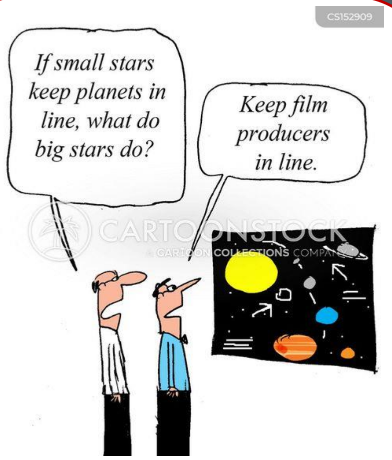

Introduction: 3C 279

- Active Galactic Nucleus (AGNs)
- Blazars – relativistic jet aligned close to the line of sight of the observer [1].

- Blazar Subclass:
  - Flat Spectrum Radio Quasars (FSRQ).
  - BL Lacertae (BL Lac).

- Target 3C 279 Characteristics:
  - FSRQ.
  - Multiwavelength variability on all timescales [2].
  - Inconsistent multi-wavelength correlation [2].

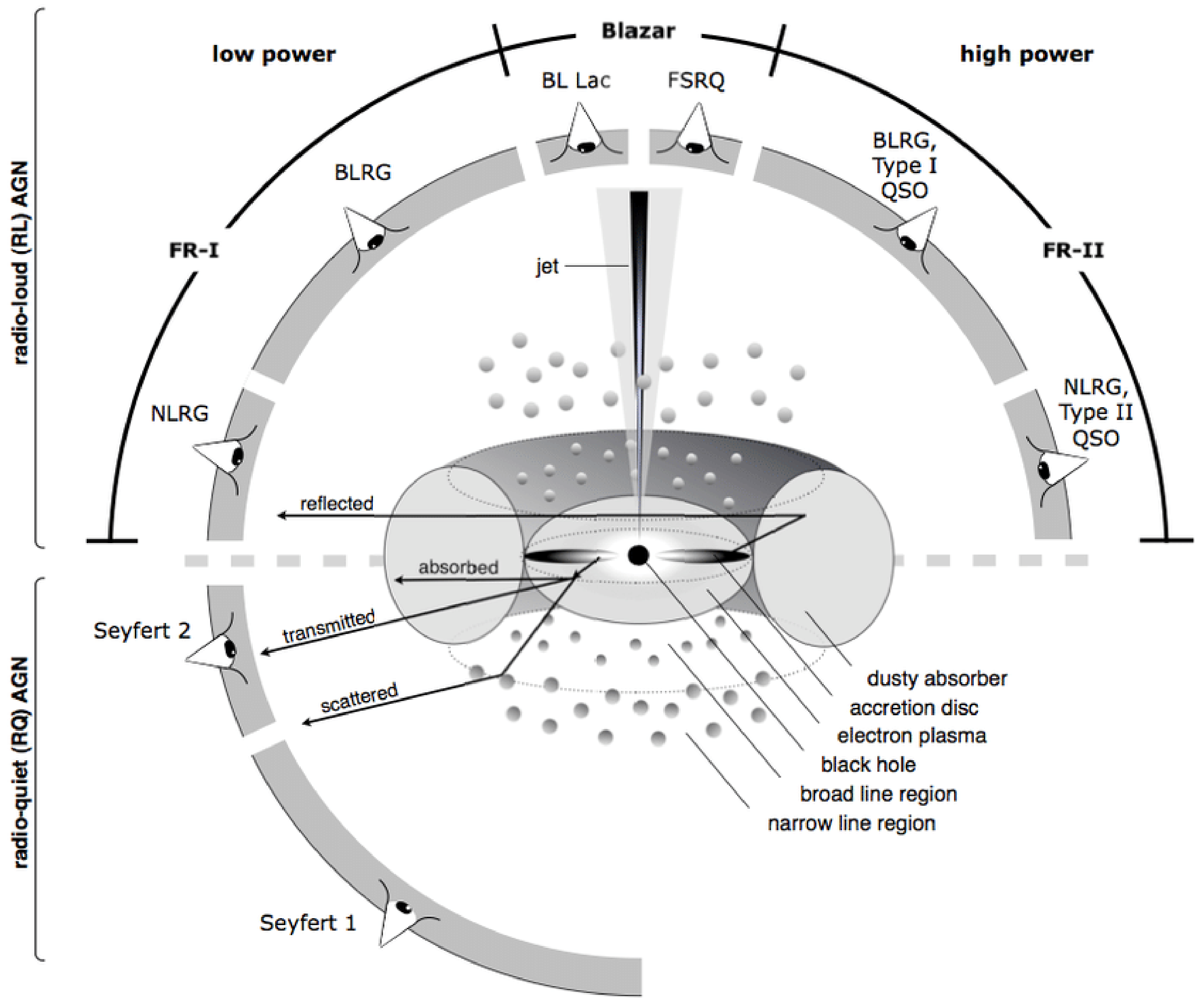

1. Beckmann, V. & Shrader, C. (2013), Active galactic nuclei, John Wiley & Sons

2. Patel, S.R., 2021. Broadband modelling of Orphan gamma ray flares. *Journal of High Energy Astrophysics*, *29*, pp.31-39.

Introduction: 3C 279

- Active Galactic Nucleus (AGNs)
- Blazars – relativistic jet aligned close to the line of sight of the observer.

- Blazar Subclass:
  - Flat Spectrum Radio Quasars (FSRQ).
  - BL Lacertae (BL Lac).

- Target 3C 279 Characteristics:
  - FSRQ.
  - Multiwavelength variability on all timescales [1].
  - Inconsistent multi-wavelength correlation [1].

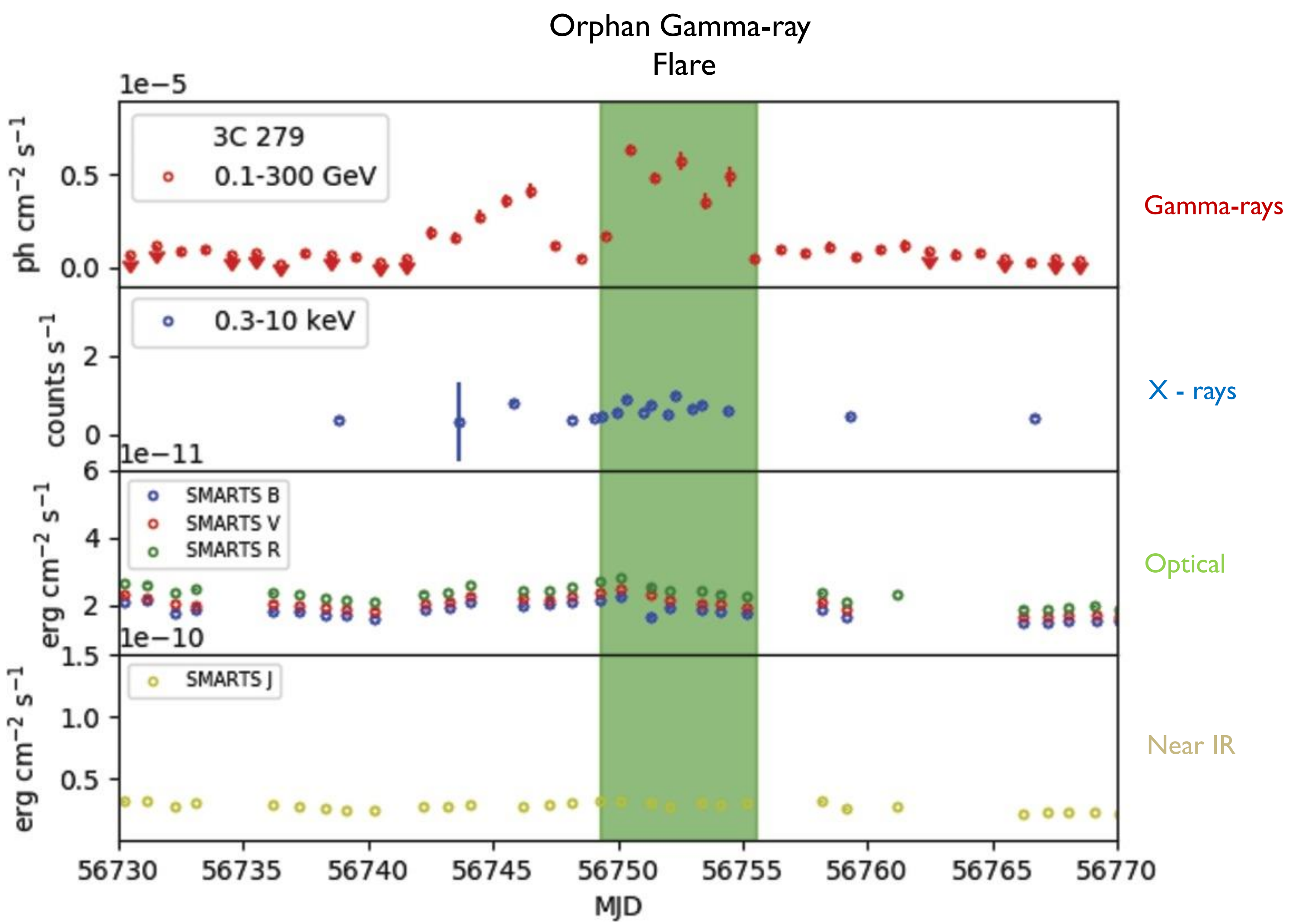

1. Patel, S.R., 2021. Broadband modelling of Orphan gamma ray flares. *Journal of High Energy Astrophysics*, *29*, pp.31-39.

Gamma-ray and Optical Correlations

- z-transformed Discrete Cross-Correlation Functions (ZDCF) [1].
  - Variability time-lags
  - To probe the number of emission zones in the jet during flares

---

- The *Fermi* Large Area Telescope (LAT): Gamma-rays 0.1 – 300 GeV [2].
  - Light-curves
  - Spectral Energy Distributions (SEDs)
- Optical Photometry:
  - Boyden Observatory: Watcher Telescope
  - Las Cumbres Observatory (LCO)
  - Steward Observatory
  - Small and Moderate Aperture Research Telescope System (SMARTS)

1. Alexander, T. (2013), 'Improved agn light curve analysis with the z-transformed discrete correlation function', arXiv preprint arXiv:1302.1508.
2. Atwood, W. (2009), 'The large area telescope on the fermi gamma-ray space telescope mission', The Astrophysical Journal 697(2), 1071.

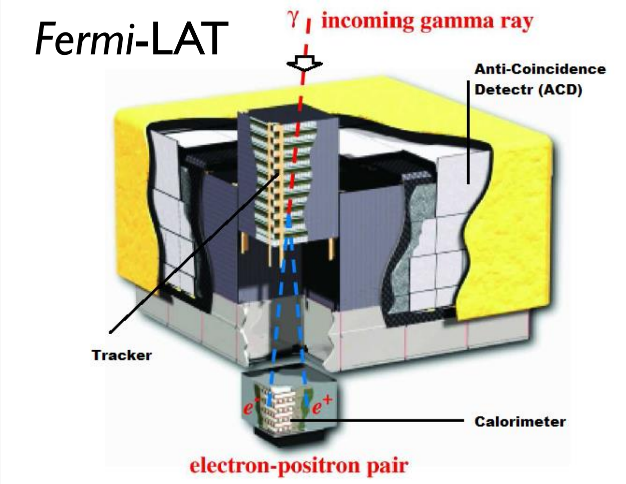

Watcher 40-cm Telescope

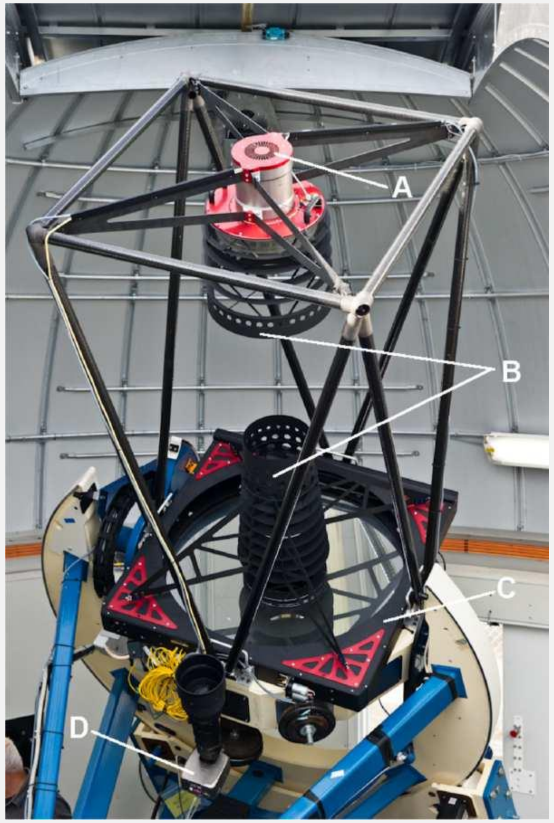

LCO 1.0-m Telescope

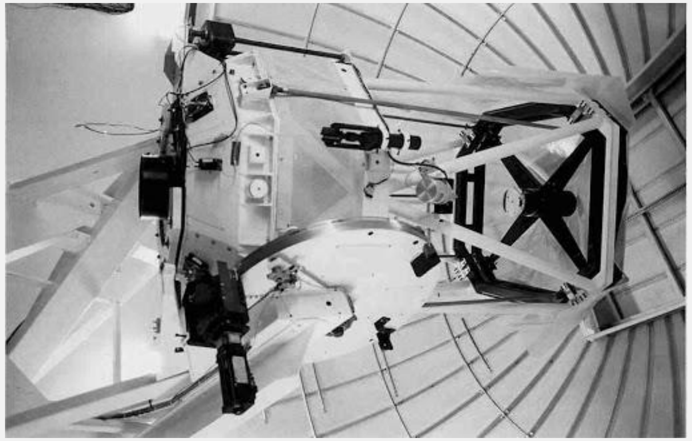

SMARTS 1.3-m Telescope

Steward Observatory

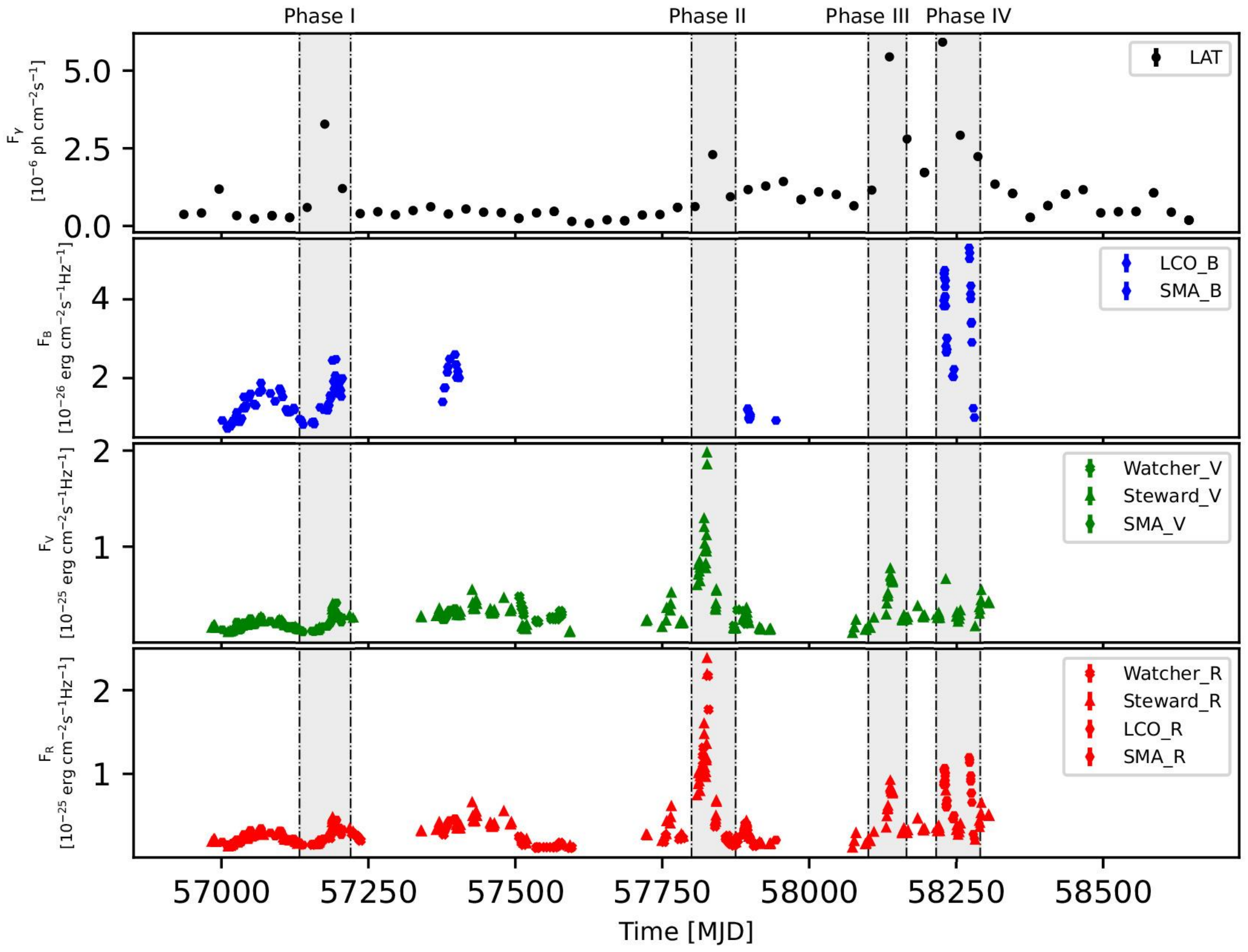

Figure 1: The gamma-ray [photon.cm^{-2}.s^{-1}] and optical [erg.cm^{-2}.s^{-1}.Hz^{-1}] light-curves of 3C 279 between 2014 – 2019.

1. Vaughan, S., (2003), ‘On characterizing the variability properties of x-ray light curves from active galaxies’, Monthly Notices of the Royal Astronomical Society 345(4), 1271–1284.

3C 279: Optical & Gamma-ray Variability

$$F_{var} = \sqrt{\frac{(S^2 - f^2_{err})}{f^2_{avg}}} \quad (1)$$

S^2 is the flux variance, f^2_{err} the mean square flux error and f^2_{avg} is the mean square flux [1].

Table 1. Observational dates and the flux variability amplitudes of the flaring phases.

Phase	MJD	Year	F_{var}
I	57180 - 57196	2015	0.96±0.02
II	57800 - 57865	2017	0.54±0.01
III	58100 - 58160	2017	0.97±0.01
IV	58216 - 58250	2018	0.69±0.05

Optical and Gamma-ray Correlations

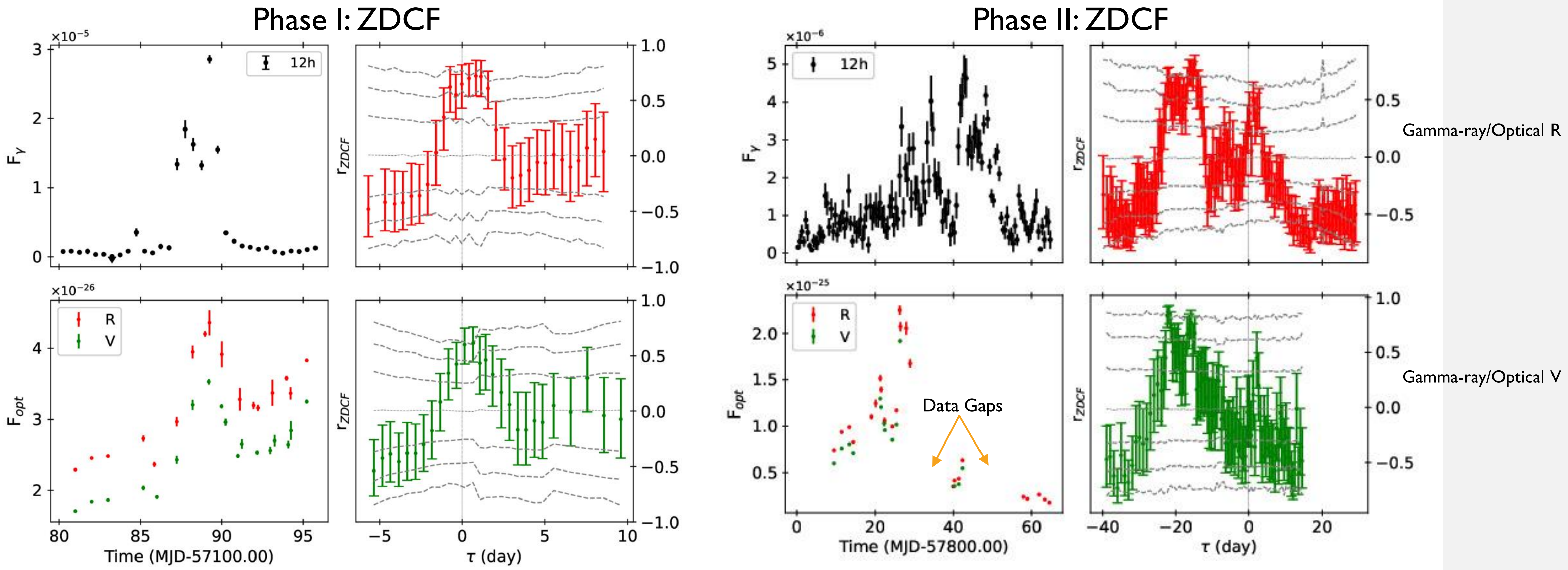

Table 2. z-transformed Discrete Cross-Correlation Functions and time-lags from Phase I and II.

Light-curves	Phase I		Phase II	
	r_{ZDCF}	τ (days)	r_{ZDCF}	τ (days)
Gamma-ray/Optical V	0.61±0.14	0.65±0.11	0.86±0.07	-21.85±0.03
Gamma-ray/Optical R	0.72±0.18	0.82±0.14	0.81±0.08	-14.82±0.09

- r_{ZDCF} peak ≥ 2σ C.L.
- Phase I:
  - The gamma-ray leads the optical ($\tau > 0$).
  - $\tau < 1$ day, i.e. near zero time-lags.
- Phase II:
  - The gamma-ray lags the optical ($\tau < 0$).
  - Two to three weeks delays (τ).

Optical and Gamma-ray Correlations

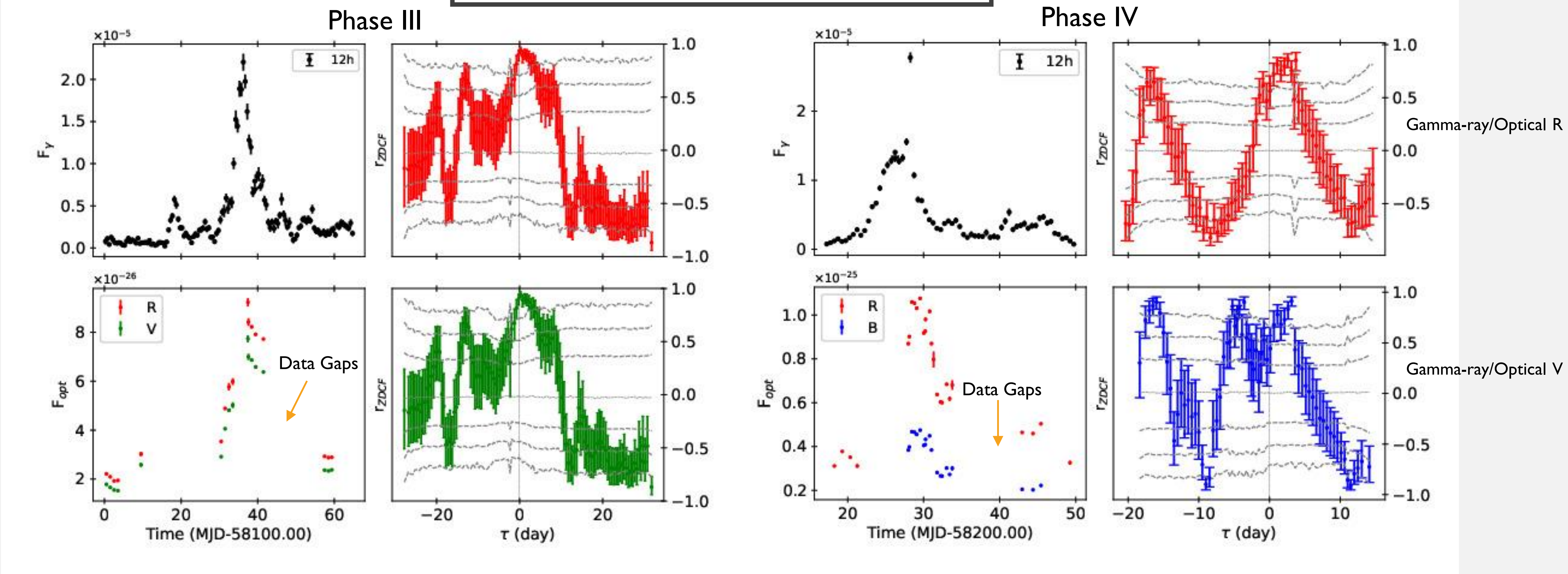

Table 3. z-transformed Discrete Cross-Correlation Functions and time-lags from Phase III and IV.

Light-curves	Phase III		Phase IV	
	r_{ZDCF}	τ (days)	r_{ZDCF}	τ (days)
Gamma-ray/Optical B	-	-	0.91±0.05	3.12±0.11
Gamma-ray/Optical V	0.94±0.03	0.23±0.02	-	-
Gamma-ray/Optical R	0.94±0.03	0.23±0.02	0.85±0.07	3.73±0.05

- r_{ZDCF} peak ≥ 3σ C.L.
- Phase III:
  - The gamma-ray leads the optical ($\tau > 0$).
  - $\tau \sim 0$ day, i.e. near zero time-lags.
- Phase IV:
  - The gamma-ray leads the optical ($\tau > 0$).
  - $\tau \sim 3 - 4$ days, i.e. near zero time-lags.

The Gamma-ray Flux Temporal Profiling & Photon Energies

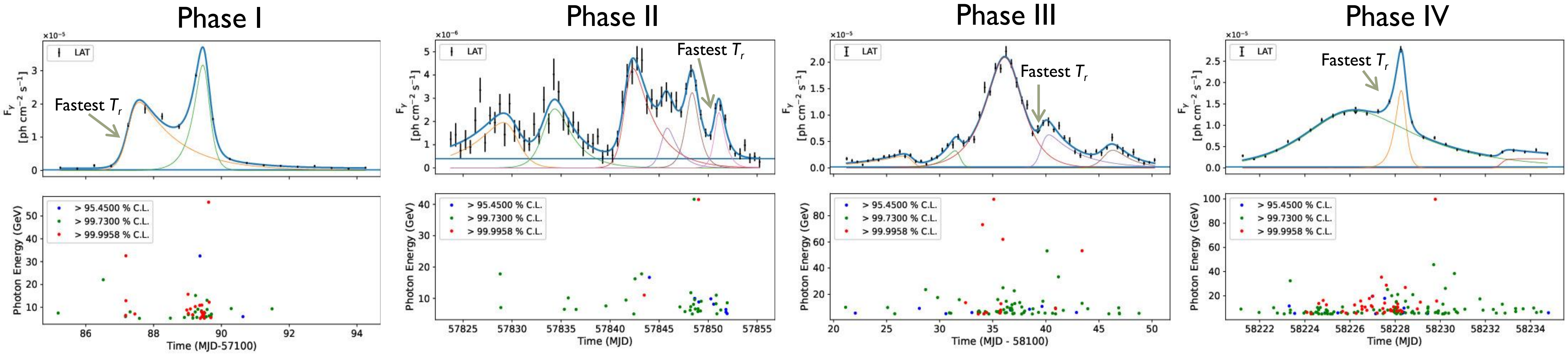

$$F(t) = F_C + 2F_0(e^{t_0 - t/T_r} + e^{t - t_0/T_f})^{-1} \quad (2)$$

- F_0 is the flare amplitude
- F_c is the constant baseline flux
- t_0 is the approximate time at F_0
- T_r is the flux rise timescale
- T_f is the flux decay timescale

$$t_d = \ln 2 \times Tr \quad (3)$$

- t_d is the flux doubling time, i.e., the time it takes the observed flux to increase by a factor two [1].

Table 4. *The gamma-ray flux temporal profiling & high energy photons from the most rapid flares during Phases I – IV.*

	T_r (days)	T_f (days)	t_d (hours)	E_γ (GeV)
I	0.16±0.02	1.18±0.07	2.66±0.33	56.00
II	0.36±0.15	0.61±0.16	5.99±2.50	41.61
III	0.32±0.13	2.99±0.81	5.32±2.16	92.22
IV	0.29±0.12	0.15±0.08	4.82±2.00	99.76

- *Asymmetric flaring profiles.*
- *Faster flux rise than decay times $T_r < T_f$, Phases I – III.*
- *Faster decay than rise times $T_r > T_f$, Phases IV.*
- *Intra-day variability (IDV), i.e. $t_d \leq 24$ hours.*
- *t_d are comparable within error (2σ).*
- *High energy photons.*

1. Abdo, A. et al. (2010), 'Gamma-ray light curves and variability of bright fermi- detected blazars', The Astrophysical Journal 722(1), 520

Relativistic Beaming

Assuming the optical depth of a high energy photon with energy $\epsilon = E_\gamma/m_e c^2$ to interact with a low energy photon in photon-photon absorption is $\boldsymbol{\tau(\epsilon) = 1}$, we determined the minimum Doppler factors [1]:

$$\delta_{\min} = \left[\frac{\sigma_T d_L^2 (1+z)^2 f_X \epsilon}{4 t_d m_e c^4}\right]^{1/6} \quad (4)$$

- σ_T is the Thomson scattering cross-section.
- d_L is the luminosity distance.
- z is the cosmological redshift.
- f_X is the X-ray flux at $\epsilon = {}^{E_\gamma}/_{m_e c^2}$.

1. Paliya, V. S. (2015), 'Fermi-large area telescope observations of the exceptional gamma-ray flare from 3c 279 in 2015 june', The Astrophysical Journal Letters 808(2), L48

Emission Region: Size & Location

By assuming the geometry of the emission regions to be spherical, we can determine their radii (**r**) and distances (*R*) relative to the SMBH [2]:

$$r \leq \frac{\delta_{\min} t_d c}{(1+z)} \quad (5)$$

$$R \geq \frac{2\delta_{\min}^2 t_d c}{(1+z)} \quad (6)$$

2. Rani et al, B. (2013), 'Radio to gamma-ray variability study of blazar s5 0716+714', Astronomy & Astrophysics 552, A11

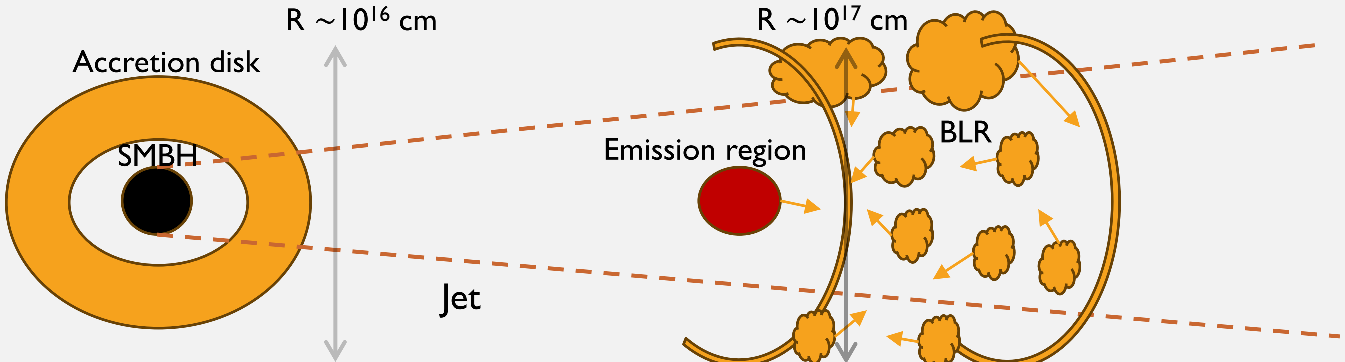

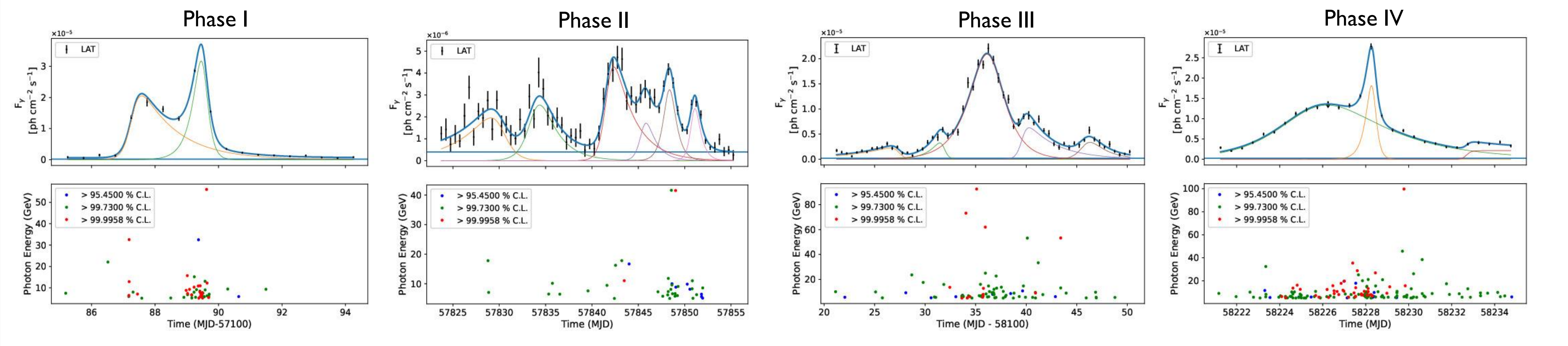

Table 5. *The minimum Doppler factors, the emission region radii and distances from the SMBH.*

	E_γ (GeV)	f_X (10^{-11}) (erg.cm^{-2}.s^{-1})	t_d (hours)	δ_{min}	r (10^{15} cm)	R (10^{17} cm)
I	33.00	5.50±0.40 [1]	2.66±0.33	16.22±0.39	3.04±0.39	0.99±0.05
II	11.02	1.56±0.33 [2]	5.99±2.50	9.57±0.75	4.03±1.71	0.77±0.13
III	53.16	6.05±0.83 [3]	5.32±2.16	15.90±1.14	6.00±2.50	1.89±0.27
IV	26.91	3.63±0.83 [3]	4.82±2.00	13.25±1.05	4.50±1.90	1.19±0.19

- Phases I, III and IV have similar relativistic beaming δ_{min} within error (2σ).
- Consistent radii r (within 1σ) for all phases.
- R is comparable with the size of the BLR, i.e., $R_{BRL} \sim 2.30 \times 10^{17}$ cm [4].

1. Pittori, C. (2015), 'Update on swift follow-up observations of the gev flaring blazar 3c 279', The Astronomer's Telegram 7668, 1.
2. Yoo, S. & An, H. (2020), 'Spectral variability of the blazar 3c 279 in the optical to x-ray band during 2009–2018', The Astrophysical Journal 902(1), 2.
3. Prince, R. (2020), 'Broadband variability and correlation study of 3c 279 during flares of 2017–2018', The Astrophysical Journal 890(2), 164.
4. Böttcher, M. & Els, P. (2016), 'Gamma–gamma absorption in the broad line region radiation fields of gamma-ray blazars', The Astrophysical Journal 821(2), 102

Gamma-ray Spectral Energy Distributions (SEDs)

$$\frac{dN}{dE} = N_0 \times \begin{cases} \left(\frac{E}{E_{\rm break}}\right)^{-\Gamma_1} \\ \left(\frac{E}{E_{\rm break}}\right)^{-\Gamma_2} \end{cases} \quad (7)$$

$\Gamma = \Gamma_1,\ E \leq E_{break}$ $\Gamma = \Gamma_2,\ E > E_{break}$

- Prefactor N_0 is in units of $MeV^{-1}cm^{-2}s^{-1}$.
- E_{break} is the break in the spectral energy
- Γ_i is the photon index below and above E_{break}.

Table 6. *Broken Power-law (BPL) likelihood fit parameters.*

Phases	N_o (10^{-10})	E_{break} (GeV)	Γ_1	Γ_2
I	1.35±0.41	0.96±0.13	1.95±0.03	2.54±0.06
II	1.11±0.26	0.70±0.08	1.95±0.03	2.43±0.03
III	0.09±0.04	1.47±0.03	2.04±0.03	2.66±0.11
IV	3.05±0.66	1.77±0.19	1.96±0.01	2.62±0.06

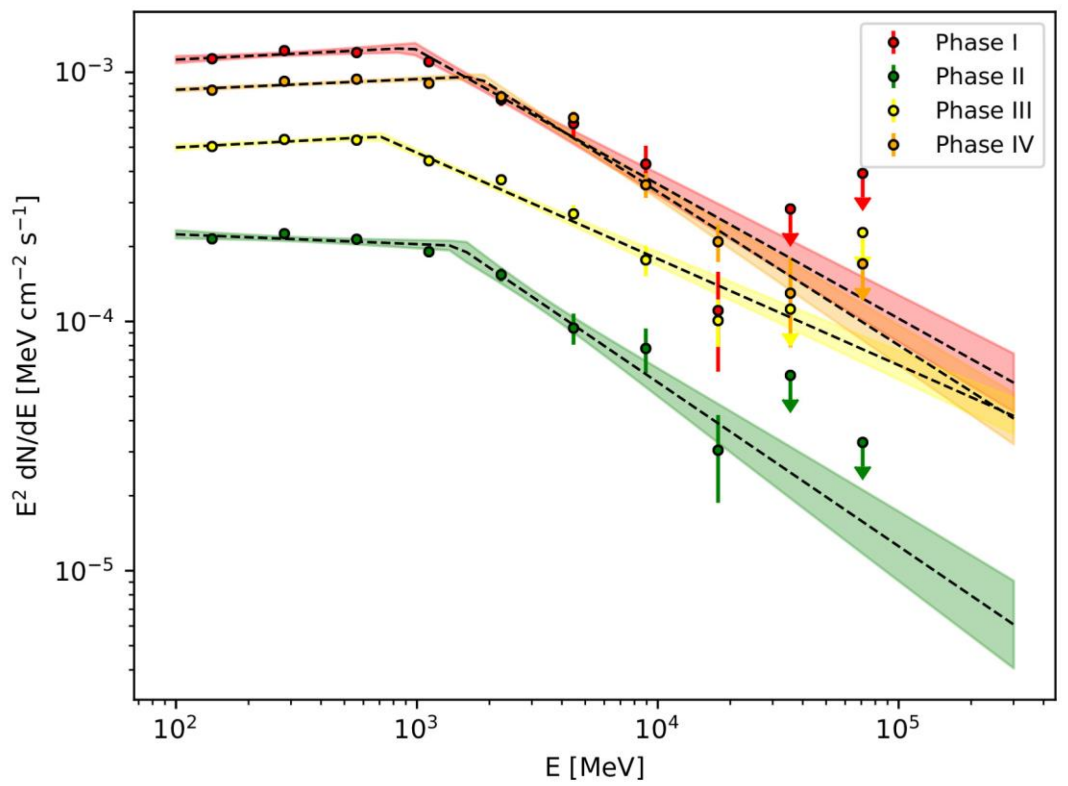

- The spectra is hard below E_{break} and softens above E_{break}.
- Phases have comparable spectral parameters.
  - Γ_i is the same within 2σ error.
  - E_{break} comparable within 3σ error.

Discussion: Emission from 3C 279

- Near zero time-lags implies that the flares were produced co-spatially by a single population of non-thermal particles.
- The emission were produced in similar emission regions, located at similar distances from the SMBH, i.e., near the outer edges of the BLR.

- Previous studies estimate external Compton cooling times in the range 7 – 27 minutes, significantly shorter than our decay times [1, 2].

- The flux rise and fall times suggest the emission were produced through interactions with standing shocks within the jet:
  - The faster rise (T_r) than decay time are consistent with the rapid injection of accelerated electrons in the emission regions at the shock front.
  - The slower decay (T_f) can be attributed to a combination of a continued injection of accelerated electrons and radiative cooling as the emission region propagates beyond the shock (Phases I, II & III).
  - The slower rise than decay observed in Phase IV could be attributed to a slow injection rate of accelerated electrons (T_r), followed by continued injection and efficient electron cooling (T_f).

1. Paliya, V. S. (2015), 'Fermi-large area telescope observations of the exceptional gamma-ray flare from 3c 279 in 2015 june', The Astrophysical Journal Letters 808(2), L48.
2. Wang, G., Fan, J., Xiao, H. & Cai, J. (2022), 'Variability and spectral behavior of gamma-ray flares of 3c 279', Publications of the Astronomical Society of the Pacific 134(1040), 104101

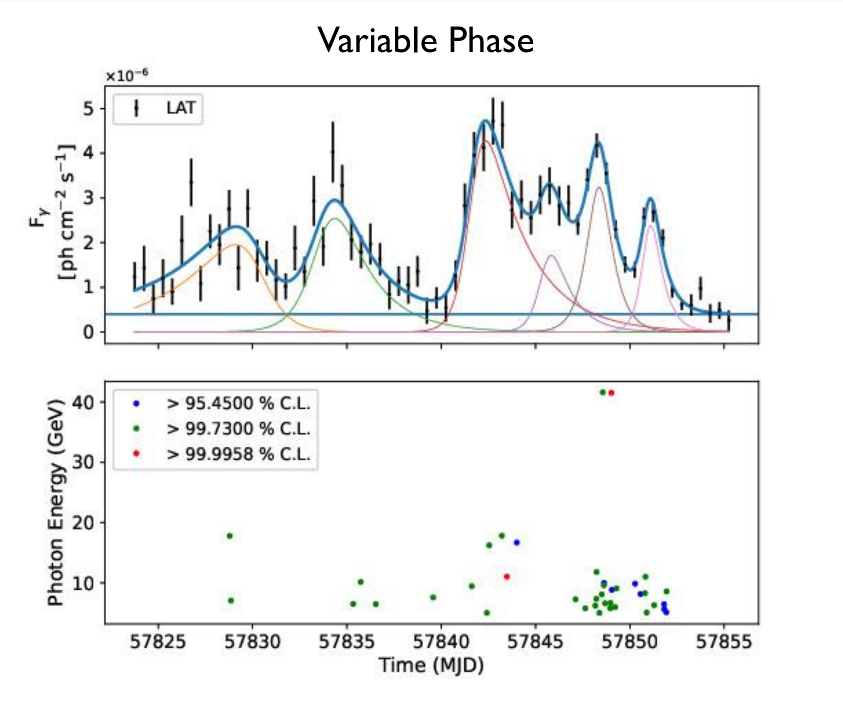

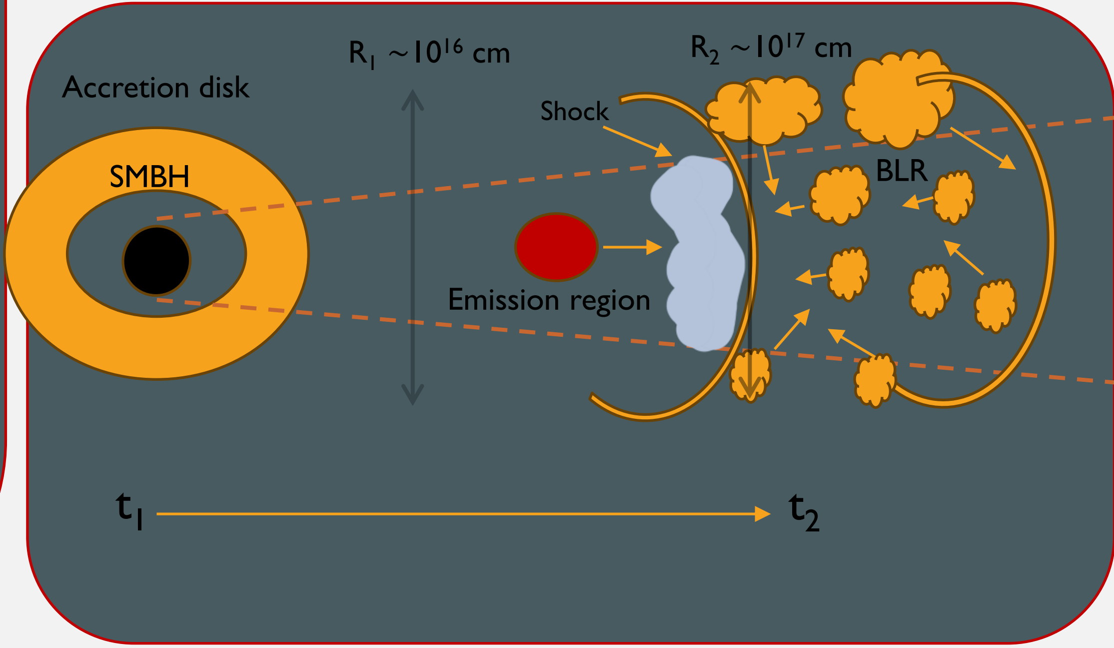

THANK YOU.